IEEE Photonics Journal
An IEEE Photonics Society Publication

Open Access

Experimental Demonstration of Coherent Combining With Tip/Tilt Control Based on Adaptive Space-to-Fiber Laser Beam Coupling

Volume 9, Number 2, April 2017

Feng Li
Chao Geng
Guan Huang
Yan Yang
Xinyang Li
Qi Qiu

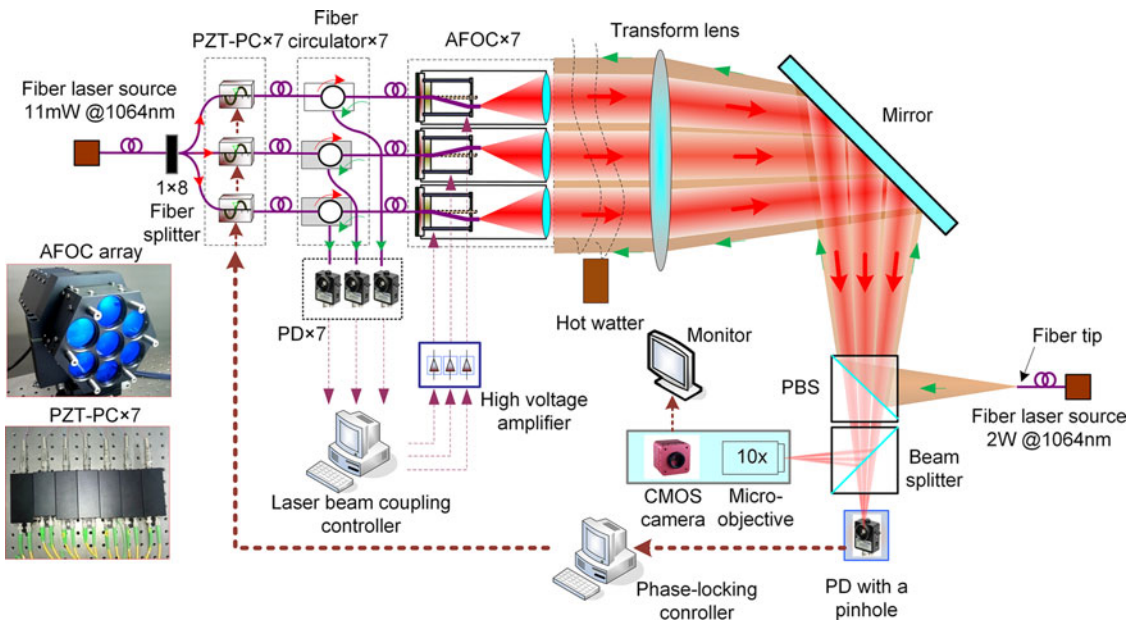

DOI: 10.1109/JPHOT.2017.2689786
1943-0655

Experimental Demonstration of Coherent Combining With Tip/Tilt Control Based on Adaptive Space-to-Fiber Laser Beam Coupling

Feng Li,[1,2] Chao Geng,[1] Guan Huang,[1] Yan Yang,[1] Xinyang Li,[1] and Qi Qiu[2]

[1]Institute of Optics and Electronics, Chinese Academy of Sciences, Chengdu 610209, China
[2]School of Optoelectronic Information, University of Electronic Science and Technology of China, Chengdu 610054, China

DOI:10.1109/JPHOT.2017.2689786

Manuscript received December 21, 2016; revised March 23, 2017; accepted March 26, 2017. Date of publication April 4, 2017; date of current version April 19, 2017. This work was supported in part by the Innovation Foundation of Chinese Academy of Sciences under Grant CXJJ-15S096 and in part by the National Natural Science Foundation of China under Grant 61675205 and Grant 61138007.
Corresponding author: Chao Geng (e-mail: blast_4006@126.com).

Abstract: A novel approach of tip/tilt control through optimizing laser beam coupling efficiencies from space to polarization-maintaining-fibers with stochastic parallel gradient descent (SPGD) algorithm for coherent beam combining (CBC) applications is proposed and demonstrated experimentally using a seven-element adaptive fiber-optics collimator (AFOC) array for the first time to the best of our knowledge. Compared with the normal target-in-the-loop SPGD method with just a single cost function, the tip/tilt control here is independent of the phase-locking control and parallel for each cell of the AFOC array. Such characteristic gives the AFOC array capacities of real-time correction of fast-changing turbulence induced tip/tilt-type phase errors. Piezoelectric-ceramic-ring fiber-optic phase compensator and AFOC are developed to correct the piston- and tip/tilt-type aberrations, respectively. The power-in-the-bucket (PIB) metric is used for phase-locking. Parallel tip/tilt control is implemented via maximizing the received power in each subaperture with fixed two-channel SPGD control. The average of normalized coupling efficiencies of seven AFOCs increases from 0.76 without tip/tilt control to 0.94 under control. In CBC, the PIB metric increases by 4.6 times, and the phase residual error is less than $\lambda/15$.

Index Terms: Active or adaptive optics, laser beam combining, laser arrays.

1. Introduction

Correction of turbulence-induced dynamic phase aberrations using adaptive optics (AO) techniques is a key objective for laser communications and beam projection applications in atmosphere. Recently developed novel fiber laser systems named as adaptive fiber laser array integrate AO with fiber optics and have inspired great research interests [1]–[9]. Compared with the customary AO-enhanced laser beam projection system with monolithic telescope, such adaptive fiber arrays are more efficient in mitigation of atmospheric turbulence effects and could generate a hit spot of the smallest possible size on the remotely located target point [10]. Phase locking on the target point, aiming at alleviating the sub-aperture averaged piston-type aberrations mainly caused by the laser

source and turbulence, is the basic item for coherent projection in atmosphere. Several techniques, like target-in-the-loop (TIL) and delayed-feed-back stochastic parallel gradient descent (DF-SPGD) [4], [5], were proposed and effectively applied in coherent beams combining (CBC) system for phase-locking over a distance of 7 km. To further promote the effect of coherent projection systems under turbulences, higher order aberrations are needed to be compensated in each sub-aperture beyond the piston errors. Such wavefront control techniques, mainly based on principle of phase-conjugate, need to install extra wavefront sensors (like Hartmann-Shack sensor) and correctors (like deformable mirror), which makes adaptive fiber array system costly, complicated and unacceptable. Recently developed adaptive fiber-optics collimator (AFOC) [3]–[16], which could be integrated into the adaptive fiber array and correct the tip/tilt-type errors, provides a promising solution to such problems. For CBC indoor, quasistatic tip/tilt errors are mainly caused by inexact assembling, vibration and thermal deformation of mechanism. While for CBC in atmosphere, turbulence-induced fast-changing tip/tilt-type errors are the hardest issues. Research results show that compensation of the tip/tilt-type errors could lead to more efficient correction of turbulence effects and results in an increase in target hit-spot brightness with even less transmitted power [2], [17], [18]. This is easy to understand because the tip/tilt-type errors take up the most part (almost 87%) [19] of the aberrations for Kolmogorov turbulence in each sub-aperture of the array.

TIL phasing with hill-climbing type techniques like SPGD [11] and multi-dithering [20] are the main existing approaches for CBC in atmosphere. In such optimization schemes, the power-in-the-bucket (PIB) metric is utilized for power-maximization, which represents the laser power backscattered by the size-limited target point. The hardest problem in such systems for tip/tilt control is the limited available bandwidth of AFOC (less than 5 kHz) [3], [7]–[9] and the slow algorithm convergence rate. It takes about 200 iterations for array with 61 sub-apertures [4], [5], [10] for phase-locking with SPGD algorithm and this value becomes twice for tip/tilt control. This means that the tip/tilt control expends more than 100 ms for optimizing and the time increases as the sub-aperture number rises. These techniques are difficult to deal with the fast-changing turbulence-induced tip/tilt aberrations with characteristic frequency close to 100 Hz [21]. The channel number of tip/tilt control is double of phase locking for the AFOC array, while the available bandwidth is much less (kHz for tip/tilt control and GHz for phase locking). That is why the hill-climbing type techniques based on single cost function are only fit for phase locking while they are not fit for tip/tilt control in long-range CBC through atmosphere.

In this paper, a novel method of sub-aperture tip/tilt control is brought up and demonstrated for CBC by experiments, for the first time to our best knowledge. Different from the conventional single metric optimization techniques, the tip/tilt control of each sub-aperture here is independent from each other, and is also independent from the phase locking control. This method promises the best use of the limited AFOC bandwidth, and the convergence keeps efficient in spite of the array scale.

In Section 2, the CBC setup of a seven sub-aperture fiber array is introduced. In Section 3, the tip/tilt control is discussed in detail. In Section 4, results of the CBC with both tip/tilt and phase-locked control are shown and discussed.

2. Experimental Setup

Fiber laser CBC experiment setup with a seven sub-aperture homemade AFOC array is illustrated in Fig. 1. Outgoing laser beams of the array come from a linearly polarized single-mode fiber laser source (NKT photonics, Koheras Adjustik) at 1064 nm wavelength with power of 11 mW and line-width of 20 kHz. The source is equally divided into eight channels by a 1×8 fiber splitter, and seven of them are employed to connect with seven piezoelectric-ceramic-ring fiber-optic phase compensator (PZT PC) separately, which will be utilized to correct the piston-type errors of the array. The homemade PZT PC, with half-wave voltage of about 1.3 V and first order resonance frequency of about 32 kHz, is produced by twisting the polarization maintaining fiber (PMF) around the piezoelectric ceramic ring. Laser beams from each PZT PC are then transmitted into seven PMF circulators and subsequently collimated by the AFOC array. The AFOC array with a hexagonal configuration is composed of seven AFOCs with a sub-aperture diameter $d = 28$ mm and adjacent

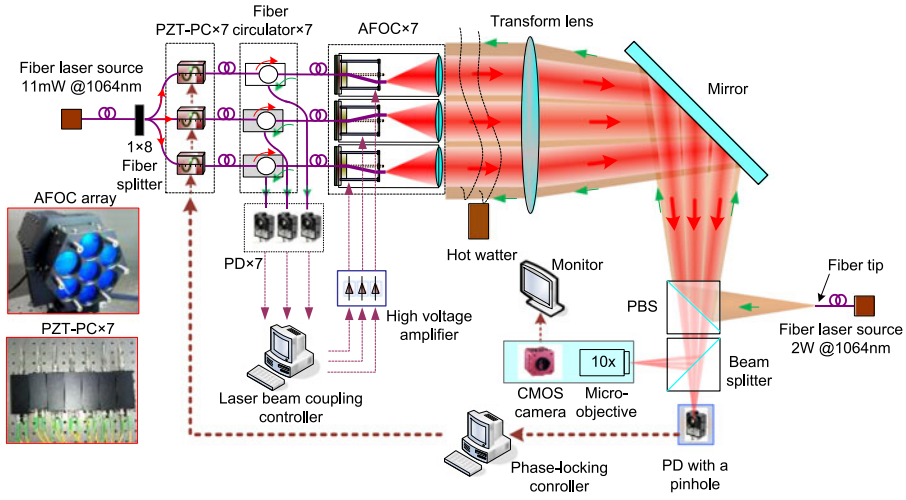

Fig. 1. Experimental setup. PZT-PC: piezoelectric-ceramic-ring fiber-optic phase compensator. AFOC: adaptive fiber-optics collimator. PD: photo detector. PBS: polarized beam splitter.

sub-aperture space of 32 mm, which decides that the filling factor of the array is equal to 0.875. The collimated outgoing beamlets are heated by hot water to bring in simulated dynamic turbulence aberrations and focused by a transform lens with a focal length of 1.5 m. Then focused beamlets are reflected by a mirror and leaded to a polarized beam splitter (PBS). Here, all of the seven beamlets are with identical polarization direction through rotating the fiber tip of each AFOC during assembling. After passing through the PBS, the focused beamlets are subsequently transmitted to another beam splitter and divided evenly into two parts. One part is sent to a photo detector (PD) with a pinhole of 20 μm diameter at the focal plane of the transform lens for phase-locking, and another part is sent to a 10$\times$ micro-objective and detected by a high-speed CMOS camera for observation. The PD is a silicon amplifier detector (PDA36A) produced by THORLABS Corporation with a 350–1100 nm response wavelength and 12.5 MHz bandwidth. A pigtail fiber end of a PMF laser source nearby the other side of the PBS is located in the focal spot of the transform lens, with wavelength of 1064 nm and optical power of about 2 W. This pigtail fiber end is used as a simulated objective in the far-filed. The output laser beam from the fiber end is reflected by the PBS and the mirror, and then collimated by the transform lens to generate a large-aperture monolithic-beam to cover the whole array. It can be found that the monolithic-beam and the seven transmitted beamlets share the same optical path and the turbulence. The monolithic-beam is cut off by the array and then focused and coupled into the PMFs of each AFOC, respectively. The coupled beamlets are separated from the outgoing beamlets through the fiber circulators and then detected by PDs.

In our setup, the SPGD algorithm is adopted to compensate the piston- and tip/tilt-type dynamic aberrations mainly caused by the hot water. PIB metric detected by the PD is used for piston control, and we call this control course phase locking (PL) here. Coupled laser power of each AFOC is employed as the metric for tip/tilt control. The tip/tilt control here is called as TT. The SPGD algorithm for PL generates seven signals to drive the seven PZT PCs. TTs of each AFOC to compensate the dynamic tip/tilt errors for both the outgoing beamlet and the coupled beamlet within the sub-apertures are parallel, and the corresponding SPGD algorithm only needs to generate two signals to actuate the AFOCs in two orthogonal directions. To our best knowledge, this is the first time CBC has been realized under simulated turbulence with parallel tip/tilt control. It should be noted that the fiber circulator employed here to separate the coupled laser beam from the outgoing laser beam can only work under power of ten-watt-level mainly subjected to current technology level. This indicates that the proposed technique here might just be utilized in low-power applications, like free space laser communication presently, where AFOC arrays are used for laser beam transceiving.

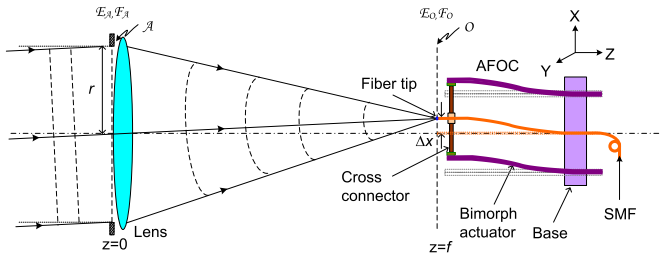

Fig. 2. Schematic diagram of coupling laser beam from free space into SMF.

The control loop of the SPGD algorithm implemented here for PL or TT is presented as follows:

1) Generate a series of random voltage perturbations (seven for PL and two for TT of each AFOC) $\delta\bar{V}$, each of which obeys the Bernoulli probability distribution with zero mean.
2) For TT, amplify the voltages $\bar{V} + \delta\bar{V}$, apply them to the AFOC on the X and Y axes separately, and get the coupled power metric P_+. For PL, apply the signal $\bar{V} + \delta\bar{V}$ on PZT PCs, and get the PIB metric P_+.
3) Apply $\bar{V} - \delta\bar{V}$ on compensators and get the corresponding metric P_-.
4) Update the applied voltages on the compensators

$$\bar{V} = \bar{V} + \xi\delta\bar{V}\,(P_+ - P_-) \tag{1}$$

where ξ is a positive value named gain coefficient of the SPGD algorithm.

5) Repeat step 1)–4) until the control progress is ended manually.

3. Tip/Tilt Control Based on Adaptive Space-to-Fiber Laser Beam Coupling

Deflecting angle of the outgoing beamlets is decided by fiber-tip's position in sub-aperture's focal plane of the AFOC. Meanwhile, turbulence-induced tip/tilt-type errors are forced the focusing speckle centroid drift in the same focal plane of AFOC for the coupling beamlets. Similar to the aberration correction based on the principle of optical phase-conjugation in AO, TT can be realized through driving the fiber-tip of the AFOC to the point where the centroid of the turbulence-influenced focusing beamlet is located in. Here, technique with adaptive beam coupling from space into a single-mode fiber (SMF) is utilized to make the fiber tip track the turbulence-induced speckle centroid drift in the sub-aperture [9], [22]. Tip/tilt phase pre-compensation for the outgoing beamlet is achieved during the adaptive beam coupling course. Adaptive fiber coupling is analyzed below.

The schematic diagram of laser beam coupling from free space into SMF of AFOC is depicted in Fig. 2. A plane wave is focused by a thin lens with aperture's radius of r and focal length of f. The lens is located at the pupil plane $\mathcal{A}$ and the SMF's tip is located in the focal plane O of the lens.

Distribution of optical beam in SMF can be approximate to a Gaussian beam within 1% error, of which the amplitude $F_O(x,\ y)$ is expressed as

$$F_O\,(x, y) = \sqrt{\frac{2}{\pi\omega_0^2}}\exp\left(-\frac{x^2+y^2}{\omega_0^2}\right) \tag{2}$$

where ω_0 is the mode field radius of the fiber core.

Displacement of the fiber tip denoted as Δx and Δy could vary as the drive voltages on the AFOC change. Corresponding backward optical field of $F_O(x,\ y)$ on plane $\mathcal{A}$ denoted as $F_A(x,\ y)$ could be calculated through Fourier transformation and expressed as

$$F_A\,(x, y) = \sqrt{\frac{2}{\pi\omega_A^2}}\exp\left(-\frac{x^2+y^2}{\omega_A^2}\right)\exp\left[\frac{j2\pi}{\lambda f}\,(x\Delta x + y\Delta y)\right] \tag{3}$$

where $\omega_A(x,\ y) = \lambda f/(\pi\omega_0)$, λ is the working wavelength, and $F_A(x,\ y)$ is normalized in aperture of the coupling lens.

Amplitude of plane wave in plane $\mathcal{A}$ is denoted as $E_A(x,\ y)$, and the corresponding amplitude of the focused laser beam in plane O is symbolized as $E_O(x,\ y)$. The tiled input plane wave laser beam could be expressed as

$$E_A\ (x, y) = E_I \exp\left\{j\frac{2\pi}{\lambda}\left[x\cos(\alpha) + y\cos(\beta)\right]\right\} \tag{4}$$

where α (or β) is the angle between the input direction and axis X (or Y). Here, it is assumed that the input field has uniform amplitude value of E_I.

Coupling efficiency denoted as η equals to the ratio of power coupled into SMF to the total power passing through the coupling lens. Coupling efficiency η could be calculated on both plane $\mathcal{A}$ and O with different expressions. Here, our analysis is based on plane $\mathcal{A}$ and η can be expressed as [22], [23]

$$\eta = \frac{\left|\iint_A E_A^*\ (x, y)\, F_A\ (x, y)\, dxdy\right|^2}{\iint_A |E_A\ (x, y)|^2 dxdy}. \tag{5}$$

Taking (3) and (4) into (5), then we get

$$\begin{aligned}\eta &= \left|\iint_{u^2+v^2\le\chi^2} \exp\left(-u^2 - v^2\right)\exp\left[j2\left(u\Delta x' + v\Delta y'\right)\right] dudv\right|^2 \\ &= \left|\frac{\sqrt{2}}{\pi\chi}\int_0^{\chi}\int_0^{2\pi} \exp\left(-r_2^2\right)\exp\left(j2r_2r_1\cos(\phi-\psi)\right) r_2 dr_2 d\psi\right|^2 \\ &= \left|\frac{2\sqrt{2}}{\chi}\int_0^{\chi} \exp\left(-r_2^2\right) J_0\left(2r_2r_1\right) r_2 dr_2\right|^2\end{aligned} \tag{6}$$

where

$$u = \frac{x}{\omega_A},\ v = \frac{y}{\omega_A},\ \chi = \frac{r}{\omega_A} \tag{7}$$

$$\Delta x' = \left(\Delta x - f\cos(\alpha)\right)\big/\omega_0,\ \Delta y' = \left(\Delta y - f\cos(\beta)\right)\big/\omega_0 \tag{8}$$

$$r_1 = \sqrt{|\Delta x'|^2 + |\Delta y'|^2},\quad r_2 = \sqrt{|u|^2 + |v|^2} \tag{9}$$

$$u = r_2\cos(\psi),\ v = r_2\sin,\ (\psi)\ \Delta x' = r_1\cos(\phi),\ \Delta y' = r_1\sin(\phi) \tag{10}$$

where $J_0(\bullet)$ is the Bessel function of the first kind and with order of zero.

Fig. 3 describes the curves of coupling efficiency. Both coupling efficiency η and optimum χ fall as r_1 increases. The maximum η is equal to 0.81 when parameter χ equals to 1.12 and r_1 is zero. In such case, Δx is equal to $f\bullet\cos(\alpha)$, and Δy equals $f\bullet\cos(\beta)$. This means that the focused spot of the titled laser beam is centered on the SMF tip of the AFOC. That is to say, driving the fiber tip of the AFOC to make it close to the focused spot is equivalent to promote the received power and correct the tip/tilt aberrations in the AFOC's aperture. Meanwhile, tip/tilt errors of the phase-conjugated outgoing laser beam is pre-compensated according to the principle of optical reciprocity.

In our system, the power loss issues due to the clipping of the outgoing laser beam by the collimator sub-aperture also needed to be taken into account when designing the structural parameters. The transmitted power-loss factor defined as τ which represents the ratio of the outgoing beam power to the total power existing on the fiber tip and could be expressed as [1]

$$\tau = 1 - \exp(-2/f_{sub}^2) \tag{11}$$

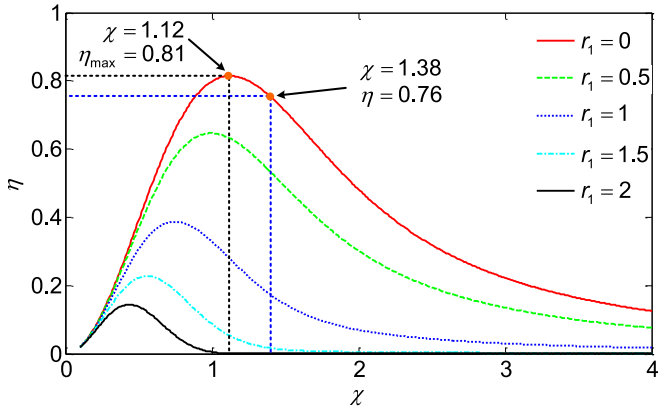

Fig. 3. Coupling efficiency curves as the function of parameter χ under different parameter r_1.

where f_{sub} is the sub-aperture's filling factor defined as $f_{sub} = \omega_a/r$, and ω_a is the outgoing Gaussian beamlet's radius and could be given by

$$\omega_a = \omega_0 \sqrt{1 + \left(\frac{\lambda f}{\pi \omega_0^2}\right)^2}. \tag{12}$$

To minimize the coupling power loss, here $f = 150$ mm is chosen. For the parameter $\omega_0 = 5\,\mu$m, the values of τ and χ are calculated to be 97.7% and 1.38. Although χ is bigger than the optimal value 1.12, the excellent coupling efficiency of 0.76 is still achieved theoretically if the tip/tilt errors are corrected.

The amplitude of the fiber tip displacement denoted as Δ is about $\pm 35\,\mu$m in any direction. The turbulence-induced focal spot displacement variation is mainly caused by the fluctuations of the wavefront angle of arrival at the sub-aperture and has standard deviation σ_F represented in the form [21]

$$\sigma_F = 0.43 f \left(\frac{d}{r_0}\right)^{\frac{5}{6}} \left(\frac{\lambda}{d}\right) \tag{13}$$

where $f = 150$ mm, $d = 28$ mm, and $\lambda = 1.064\,\mu$m in our system. In strong turbulence conditions, the Fried parameter r_0 approximates to 10 mm. Then σ_F equals to $5.8\,\mu$m and Δ equals to $6\sigma_F$, which means that the fiber tip displacement here is sufficient for the severe turbulence conditions.

The first order resonant frequency of the AFOC applied in our experiment is about 2.2 kHz and the 3-dB bandwidth is about 1.3 kHz, which is a dozen times of the characteristic frequency of the tip/tilt aberrations under atmospheric turbulence. This means that the AFOC could cope with the dynamic turbulence-induced aberrations. Meanwhile, the bandwidth of the AFOC could be multiply promoted by means of voltage filter and structure optimization.

The critical fiber parameter that could influence the coupling efficiency is the mode field radius of the fiber core, and therefore, the results of adaptive space-to-fiber laser beam coupling for PMFs and SMFs with identical fiber core size are the same. Analysis based on SMFs here also applies to PMFs utilized in our experiment setup.

4. Results and Discussion

4.1. Correction of Simulated Turbulence Aberrations Based on AFOC Array Coupling

In our system, dynamic aberrations similar to atmospheric turbulence are introduced by boiled water placed in front of the AFOC array as shown in Fig. 1. Aberrations distributed in each sub-aperture of the AFOC array contain tip/tilt-type errors and higher order aberrations. Tip/tilt-type errors cause

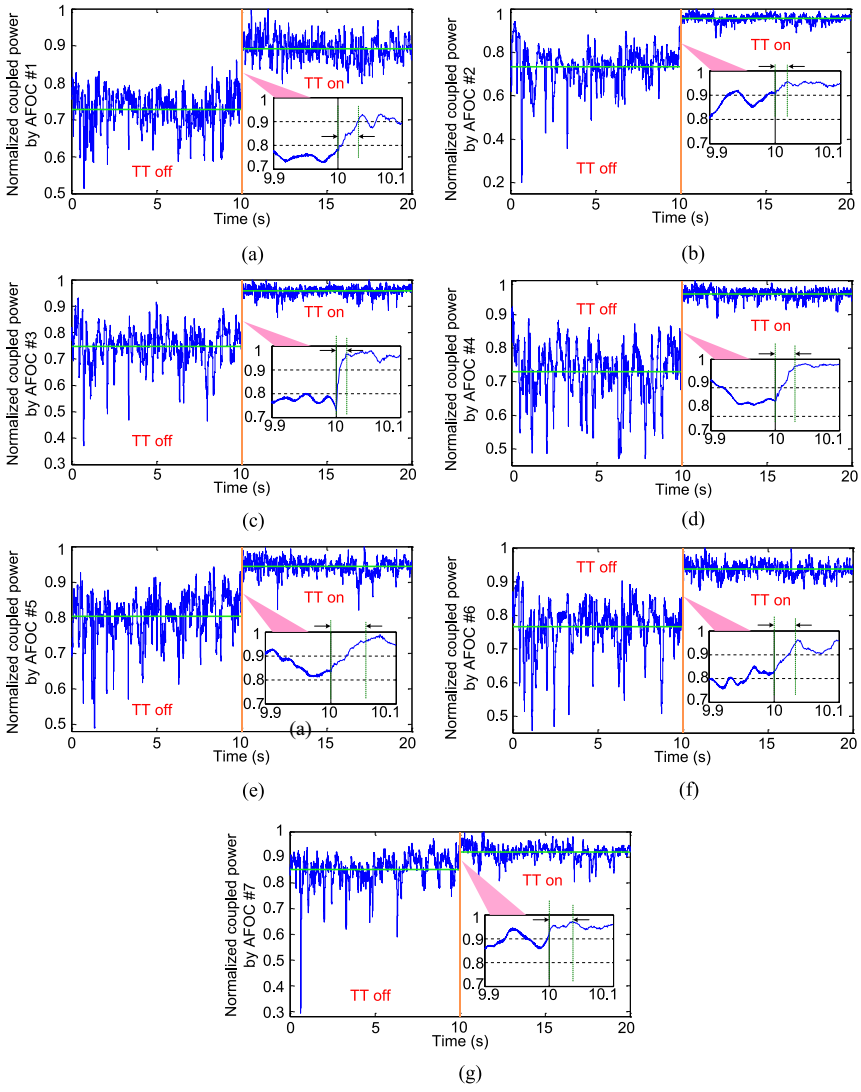

Fig. 4. Normalized coupled power curve of 20 s for each AFOC in the array. (Inset) Zoomed-in behavior of the power metric at point when the TT control is implemented.

deviation of the focused speckle from the ideal focal spot in the sub-aperture, as shown in Section 3. Higher order aberrations cause misalignment between the eigen mode of the SMF and the focused optical field. Such misalignment finally brings down the coupled power into the SMF. It should be noticed that the tip/tilt-type errors take up the predominant part of the aberrations in atmospheric turbulence and also in our system as shown below. The iteration rate of TT control is designed at 1 kHz, which is mainly restricted by the speed-limited analog-digital converter card of which the rate sharply declines as the input channel increases. The SPGD algorithm for TT control is shown in Section 2.

Fig. 4 shows the curve of the normalized coupled power under processes with and without TT control under simulated turbulence for each AFOC of the array. The coupled power is normalized via being divided by the maximum value during the whole process. The two processes last for 20 s totally and each for 10 s. When TT control is off, the coupled power of the AFOCs drifts around and the intensity is low due to the simulated turbulence. Much of the power jitter is suppressed and noticeable promotion of the power metric is achieved when the TT control is implemented. The TT control takes about 30 iterations, equivalent to 30 ms, for SPGD max-optimization. The TT control

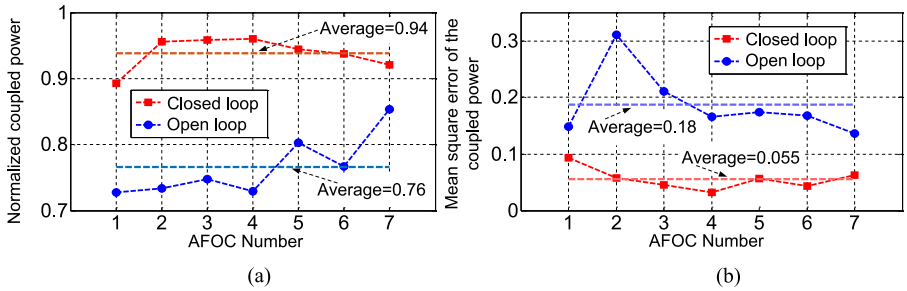

Fig. 5. Average (a) and mean square error (b) of the normalized coupled power for each AFOC when TT control is in open loop and closed loop.

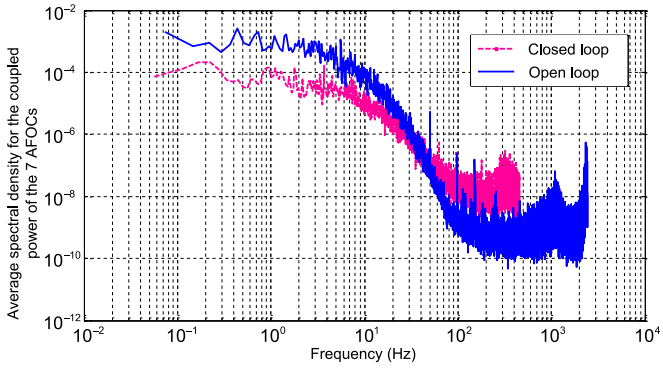

Fig. 6. Average frequency spectrum density analysis for laser power coupled by seven AFOCs.

is parallel for each AFOC, and therefore, the convergence rate will not change as the number of the array enlarges. The average normalized coupled power for all the seven AFOCs is about 0.76 without TT control and then increases to 0.94 when TT control is brought in, as shown in Fig. 5(a). The average mean square error (*MSE*) of the coupled power for all the seven AFOCs is about 0.18 in open loop and then turns to 0.055 in closed loop as illustrated in Fig. 5(b). The average frequency spectrum density curve of the normalized power of the seven AFOCs is shown in Fig. 6. The curves for TT on and TT off cross at frequency point about 38 Hz, which is corresponding to the SPGD convergence time equal to about 30 ms. It should be noticed that the coupled power is not all along locked at the maximum value when TT control is on. Limited iteration rate and higher order aberrations beyond the function of the AFOCs can explain such issues. Larger coupled power jitter corresponds to stronger aberrations. The major aberrations introduced by the boiled water are tip/tilt-type errors, which is similar to the true atmosphere turbulence. This conclusion can be inferred from the fact that the coupled power jitter with TT on is much less than that without control.

4.2. Coherent Beam Combining of the AFOC Array

After demonstrating the tip/tilt control based on AFOC array coupling, the experiment of CBC under simulated turbulence is carried out with both piston- and tip/tilt-type phase error correction. PIB metric acquired by the PD placed on the focal spot of the transform lens, as show in Fig. 1, is used as the SPGD metric to compensate the piston-type errors and such control is called as PL here. The iteration rate of the PL is about 12 kHz. The SPGD algorithm for PL is shown in Section 2. Fig. 7 shows the normalized PIB metric acquired from the PD as the function of time during four stages, which are no control stage, PL stage, PL and TT stage, and single TT stage. Each of the four stages lasts 5 s. The first two stages are corresponding to the TT on process in part A of Section 4 and the last two stages to the TT off process. The PIB metric is normalized via being divided by the maximum PIB during the four stages. When no control is under operation, the mean

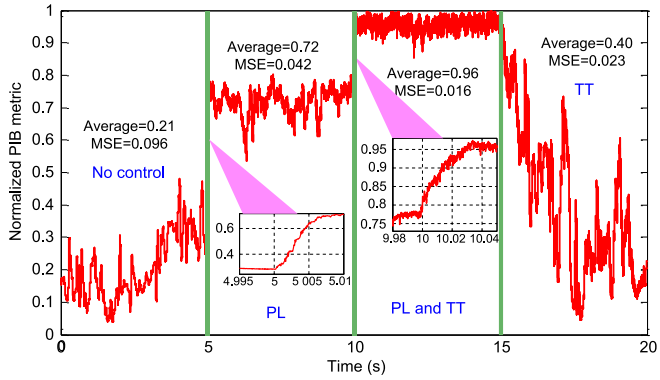

Fig. 7. Normalized PIB metrics acquired by PD as the function of time.

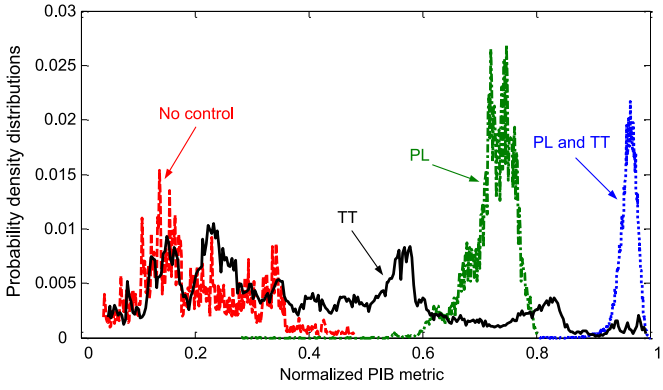

Fig. 8. Histogram (probability density distribution) of the PIB metrics normalized by the maximum PIB metric.

PIB metric is only 0.21 and the *MSE* of the metric is 0.096, which is mainly caused by the simulated turbulence and the phase noise induced by the transmission fibers. When PL control is on and TT control is off, the normalized PIB metric is locked at a higher value with an average of 0.72, which is 3.4 times of that for no control stage. The *MSE* decreases to 0.042. The PIB metric convergence procedure with sole PL control takes only about 7 ms.

Subsequently, the TT control is brought in and the PIB metric is further optimized. The metric is with an average of 0.96 and *MSE* of 0.016, which is only 1/6 of that in the no control stage. The convergence of the adaption process after the TT control is switched on takes time about 30 ms, which equals to the time that each AFOC needs to maximize the coupled power in part A of Section 4. Such results indicate that the technique illustrated in Section 3 realizes the parallel tip/tilt control for each AFOC, and such control is independent from the phase locking, which is quite different from the existing techniques.

A residual phase error is evaluated to be less than $\lambda/15$ using expression [24]

$$\Delta\phi_{rms} = 2\sqrt{\Delta P_{rms}/P_{\max}} \tag{14}$$

where P is the PIB metric evolution when CBC is achieved.

Finally, the TT goes on while the PL is shut down. The average of the PIB metric falls to 0.40 and the *MSE* increases to 0.023. The transition from the no control stage to the TT stage shows that compensation of tip/tilt-types errors in each sub-apertures results in relatively small PIB metric promotion without compensation for piston-type aberrations.

The metric histograms computed according to the results corresponding to each of the four operation stages are presented in Fig. 8. These histograms indicate the probability density distribution

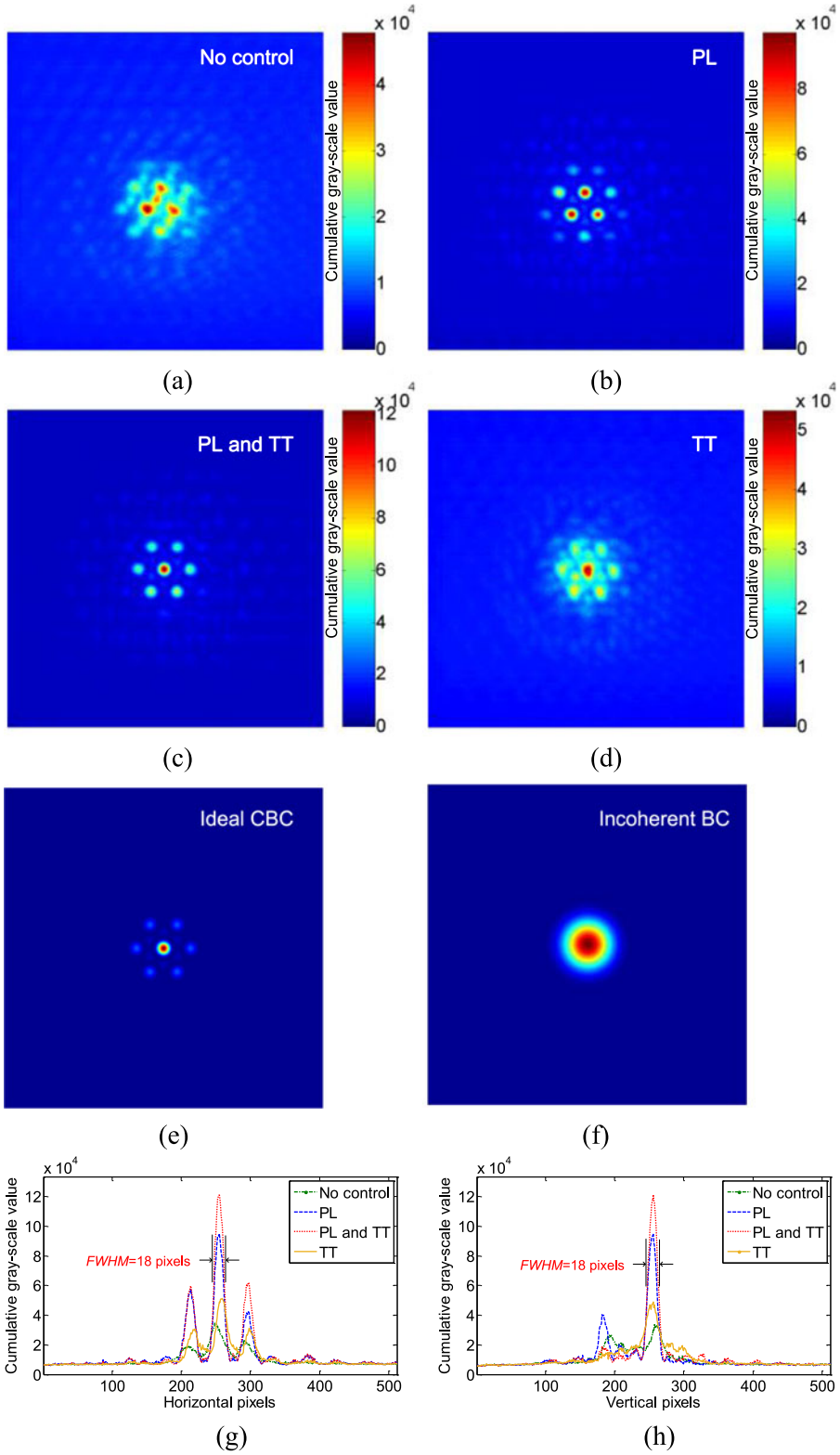

Fig. 9. Long-exposure far-field intensity distributions acquired by the CMOS camera. (a) No control. (b) PL control. (c) PL and TT control. (d) TT control. (e) Theoretical results of ideal CBC. (f) Theoretical results of ideal incoherent BC. (g) and (h) One-dimensional intensity distributions of (a)–(d) along the horizontal and vertical central lines, respectively.

of the PIB metrics. Bigger width of the histogram curves indicates higher fluctuation level of the metric. The metric at the central point of the histogram curve corresponds to the mean value. The histogram of the no control stage is highly wavy and broad. Such a result indicates that the focal spot of the laser beams from the AFOCs is unstable, which is mainly caused by the simulated dynamic aberrations and the random phase noises in the fiber system. The histogram curve acquired during the adaptation process of the PL control is transformed to larger value area. Most of all, the width of the curve is notably compressed and this indicates that the focal spot is much more stable. Further compensation of the tip/tilt-type errors results in noticeable performance promotion, where the metric is bigger and the histogram curve is narrower. This means that the focal spot is further stabilized. Most part of the TT histogram distributes in range of larger metric compared with the no-control histogram. But the metric fluctuations of the TT are higher, which can be inferred from the fact that the TT histogram is wider and has several peak-values.

The long-exposure far-field intensity distributions during the four control stages are shown in Fig. 9(a)–(d), respectively. The frame frequency of the camera is about 120 Hz with window of 512 $\times$ 512 pixels and max gray-scale value of 256 (8-bit depth). Image grabbing was started at the beginning of each stage and images were accumulated until this stage was ended. When no control is implemented, the long-exposure pattern is diffused by the simulated turbulence, and the fringe visibility is very weak. When PL control is implemented, fringe contrast increases and the results similar to the ideal pattern [see Fig. 9(e)] are achieved. Nevertheless, intensity of the side lobes located bellow the main lobe approximates that of the main lobe, which is much different from the theoretical results. This can be attributed to two reasons. One is that the simulated turbulence breaks apart the outgoing laser beams. The other is that the initial static pointing errors of the AFOCs during assembling deflect the overlap point from the pinhole used for PL control. Additional pre-compensation of the tip/tilt-type errors through the TT control could resolve such issues and results in pattern [see Fig. 9(c)] comparable with the ideal pattern [see Fig. 9(e)]. Sole TT control just benefits the intensity of the central point, but not the fringe contrast [see Fig. 9(d)], but this control still gains results which surpass the incoherent beam combining [see Fig. 9(f)]. Fig. 9(g) and (d) are the 1-D intensity distributions of Fig. 9(a)–(d), along the horizontal and vertical central lines, respectively. The full width at half maximum (FWHM) of the main lobe takes up about 18 pixels, which equals about 194 μm (10.8 μm for each pixel). The true FWHM value is 19.4 μm after divided by the amplification ratio of the 10$\times$ micro-object. This value is suitable for the size of the 20 μm diameter pinhole which is placed before the PD to acquire the PIB metric, as discussed above.

5. Conclusion

We have demonstrated the effectiveness of this novel fiber–coupling-based tip/tilt control method through CBC experiments with a seven-elment AFOC array. Compared with the customary TIL SPGD method with just a single metric, the tip/tilt control here is independent of the phase-locking control and parallel for each cell of the AFOC array. Such characteristic gives the AFOC array abilities of real-time correction of fast-changing tip/tilt-type phase errors, especially for the turbulence-induced fluctuations of the wavefront angle of arrival at the AFOC's aperture. PZT PC and AFOC are developed to compensate the piston- and tip/tilt-type aberrations, respectively. The PIB cost function is used for phase-locking and the laser beam coupling optimization is employed for parallel tip/tilt control via maximization of the coupled power in each aperture with fixed two-channel SPGD control. The average of normalized coupling efficiency of the AFOC array increases from 0.76 without tip/tilt control to 0.94 under control. In CBC, the PIB metric increases by 4.6 times, and the phase residual error is less than λ/15.

The pigtail fiber-end used as a simulated objective in the far-filed in our experimental setup is just for research convenience, not required for real atmosphere CBC applications. Actually, the function of this fiber-end is similar to the beacon used to deliver the turbulence aberration information in traditional AO system. For cooperative-target CBC applications with AFOC array, e.g., free space laser communications, such fiber-end could be replaced by a corner-cube-prism or bright light

source. For non-cooperative target, light reflected by the target surface could act as the beacon, but that is a quite different and difficult topic. Meanwhile, coupled laser power of the AFOC array could be also utilized as the TIL PIB metric if a corner-cube-prism was set at the target point, and therefore, an additional receiving telescope might be not needed.

The method proposed above will be further improved and expanded, and the CBC experiments in real atmosphere based on hardware will be performed in the near future.

References

[1] M. A. Vorontsov and S. L. Lachinova, "Laser beam projection with adaptive array of fiber collimators. I. Basic considerations for analysis," *J. Opt. Soc. Amer. A*, vol. 25, no. 8, pp. 1949–1959, Aug. 2008.

[2] S. L. Lachinova and M. A. Vorontsov, "Laser beam projection with adaptive array of fiber collimators. II. Analysis of atmospheric compensation efficiency," *J. Opt. Soc. Amer. A*, vol. 25, no. 8, pp. 1960–1973, Aug. 2008.

[3] M. A. Vorontsov, T. Weyrauch, L. A. Beresnev, G. W. Carhart, L. Liu, and K. Aschenbach, "Adaptive array of phase-locked fiber collimators: analysis and experimental demonstration," *IEEE J. Sel. Topics Quantum Electron.*, vol. 15, no. 2, pp. 269–280, Mar./Apr. 2009.

[4] T. Weyrauch *et al.*, "Experimental demonstration of coherent beam combining over a 7 km propagation path," *Opt. Lett.*, vol. 36, no. 22, pp. 4455–4457, Nov. 2011.

[5] T. Weyrauch *et al.*, "Deep turbulence effects mitigation with coherent combining of 21 laser beams over 7 km," *Opt. Lett.*, vol. 41, no. 4, pp. 840–843, Feb. 2016.

[6] M. A. Vorontsov, S. L. Lachinova, L. A. Beresnev, and T. Weyrauch, "Obscuration-free pupil-plane phase locking of a coherent array of fiber collimators," *J. Opt. Soc. Amer. A*, vol. 27, no. 11, pp. A106–A121, Nov. 2010.

[7] C. Geng, W. Luo, Y. Tan, H. Liu, J. Mu, and X. Li, "Experimental demonstration of using divergence cost-function in SPGD algorithm for coherent beam combining with tip/tilt control," *Opt. Exp.*, vol. 21, no. 21, pp. 25045–25055, Oct. 2013.

[8] C. Geng *et al.*, "1.5 kW incoherent beam combining of four fiber lasers using adaptive fiber-optics collimator," *IEEE Photon. Technol. Lett.*, vol. 25, no. 13, pp. 1286–1289, Jul. 2013.

[9] F. Li, C. Geng, X. Li, and Q. Qiu, "Co-aperture transceiving of two combined beams based on adaptive fiber coupling control," *IEEE Photon. Technol. Lett.*, vol. 27, no. 17, pp. 1787–1790, Sep. 2015.

[10] M. A. Vorontsov *et al.*, "Comparative efficiency analysis of fiber-array and conventional beam director systems in volume turbulence," *Appl. Opt.*, vol. 55, no. 15, pp. 4170–4185, May 2016.

[11] M. A. Vorontsov and V. P. Sivokon, "Stochastic parallel-gradient-descent technique for high-resolution wavefront phase-distortion correction," *J. Opt. Soc. Amer. A*, vol. 15, no. 10, pp. 2745–2758, Oct. 1998.

[12] L. Liu, M. A. Vorontsov, E. Polnau, T. Weyrauch, and L. A. Beresnev, "Adaptive phase-locked fiber array with wavefront phase tip-tilt compensation using piezoelectric fiber positioners," *Proc. SPIE*, vol. 6708, pp. 1–12, 2007.

[13] C. Geng, X. Li, X. Zhang, and C. Rao, "Coherent beam combination of an optical array using adaptive fiber optics collimators," *Opt. Commun.*, vol. 284, no. 24, pp. 5531–5536, Sep. 2011.

[14] D. Zhi, P. Ma, Y. Ma, X. Wang, P. Zhou, and L. Si, "Novel adaptive fiber-optics collimator for coherent beam combination," *Opt. Exp.*, vol. 22, no. 25, pp. 31520–31528, Dec. 2014.

[15] D. Zhi, Y. Ma, Z. Chen, X. Wang, P. Zhou, and L. Si, "Large deflection angle, high-power adaptive fiber optics collimator with preserved near-diffraction-limited beam quality," *Opt. Lett.*, vol. 41, no. 10, pp. 2217–2220, May 2016.

[16] X. Wang *et al.*, "350-W coherent beam combining of fiber amplifiers with tilt-tip and phase-locking control," *IEEE Photon. Technol. Lett.*, vol. 24, no. 19, pp. 1781–1784, Oct. 2012.

[17] S. L. Lachinova and M. A. Vorontsov, "Performance analysis of an adaptive phase-locked tiled fiber array in atmospheric turbulence conditions," *Proc. SPIE*, vol. 5895, pp. 1–14, 2005.

[18] G. A. Filimonov, M. A. Vorontsov, and S. L. Lachinova, "Performance analysis of a coherent tiled fiber-array beam director with near-field phase locking and programmable control of tip/tilt and piston phases," *Proc. SPIE*, vol. 8971, no. 9, pp. 1–6, 2014.

[19] R. J. Noll, "Zernike polynomials and atmospheric turbulence," *J. Opt. Soc. Amer.*, vol. 66, no. 3, pp. 207–211, Oct. 1976.

[20] Y. Ma *et al.*, "Coherent beam combination of 1.08 kW fiber amplifier array using single frequency dithering technique," *Opt. Lett.*, vol. 36, no. 6, pp. 951–953, Mar. 2011.

[21] J. W. Hardy, *Adaptive Optics for Astronomical Telescope*. New York, NY, USA: Oxford Univ. Press, 1998.

[22] W. Luo *et al.*, "Experimental demonstration of single-mode fiber coupling using adaptive fiber coupler," *Chin. Phys. B*, vol. 23, no. 1, pp. 014207-1–014207-6, 2014.

[23] H. Takenaka, M. Toyoshima, and Y. Takayama, "Experimental verification of fiber-coupling efficiency for satellite-to-ground atmospheric laser downlinks," *Opt. Exp.*, vol. 20, no. 14, pp. 15301–15308, Jul. 2012.

[24] L. Lombard *et al.*, "Coherent beam combination of narrow-line width 1.5 μm fiber amplifiers in a long-pulse regime," *Opt. Lett.*, vol. 36, no. 4, pp. 523–525, Feb. 2011.